The emergence of memory in liquid crystals

The nematic phase of liquid crystals (LC), used in most LC display applications, is a fluid state formed by orientationally ordered molecules. The direction of their alignment, and hence the overall optical response of the material, is easily modified by the application of an electric field and elastically relaxes back to a well-defined off-state when the field is removed. It has been recently shown that hybrid materials formed by nematic LCs incorporated in complex micro-structured porous matrices are often capable of indefinitely retaining the alignment direction imposed by an electric field. Such multistability is ultimately due to the interactions of the porous material with the lines of topological defects that develop within the confined nematic. Controlling the defect lines and their interactions is crucial to the design of materials whose optical properties are electrically driven but spontaneously preserved.

Francesca Serra, Marco Buscaglia, and Tommaso Bellini*
Dipartimento di Chimica, Biochimica, Biotecnologie per la Medicina, Università di Milano, Milano, Italy
*E-mail: tommaso.bellini@unimi.it

Current liquid crystal displays exploit the anisotropy, flexibility, and elasticity of the long-ranged molecular ordering of the nematic phase. Because of the intrinsic fluidity and the dielectric uniaxiality, the orientation of a nematic liquid crystal (NLC) within a pixel is readily controlled by an electric field E[1]. In turn, the direction of molecular alignment affects the polarization state of transmitted light, thus determining the *on* and the *off* state of each pixel. Upon removal of the field, the weak elasticity of nematics drives the pixel back to its off-state, which is a stable, unique, and well-defined state determined by the cell surface alignment. In Fig. 1a and 1b two of the most common schemes used in commercial displays are shown: twisted nematics[2] (TN)

and in-plane switching[3,4] (IPS), respectively. An alternative concept for display technology is the use of bistable or multistable materials, in which the electric field is needed to switch the system between two or more states that remain stable without the need for a continuous supply of energy. Several solutions for nematic-based bistable devices have been investigated over the last 30 years, without offering, so far, a practical alternative to the dominant technology used in conventional flat displays. However, the e-book concept and similar applications requiring a refreshable printed paper-like display without an embedded illumination source, is stimulating interest in new multistable display concepts.
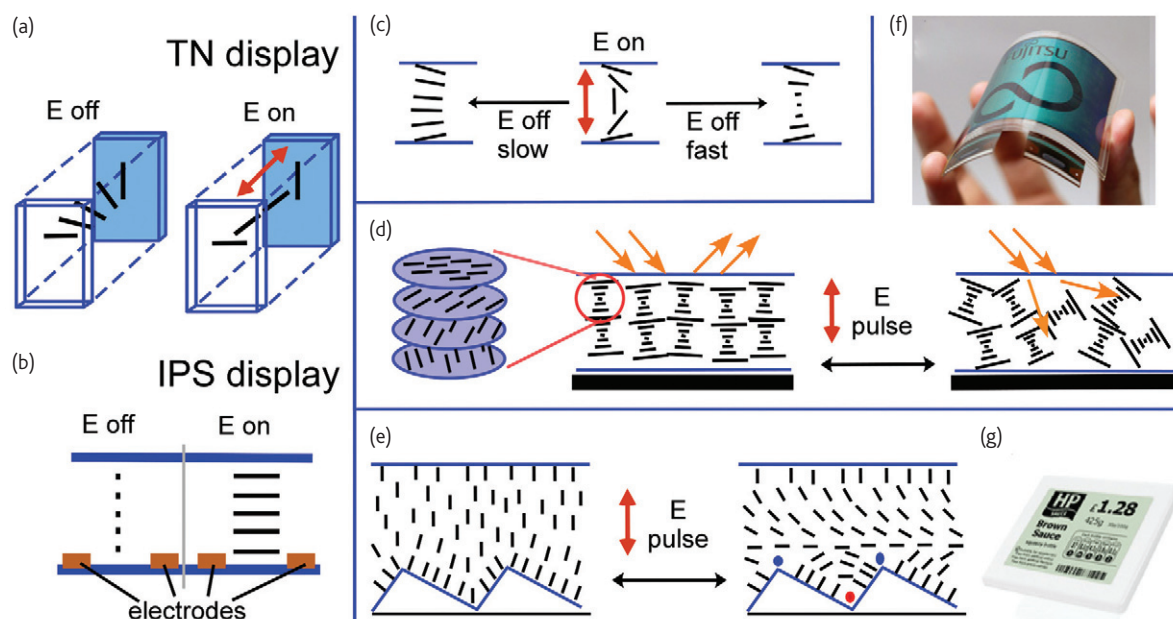
Fig. 1 Mono and bistable nematic displays. (a,b) Schemes of common monostable displays: (a) TN and (b) IPS. Black dashes represent NLCs, indicating their average orientation. (c–g) Bistable NLC devices, based either on (c, d) chiral phases or on (e) patterned surfaces. Scheme of the chiral nematic ordering is shown in violet. Some bistable displays are commercially available, such as (f) the flexible e-paper by Fujitsu (courtesy of Fujitsu) and (g) the Epop display by ZBD. (Courtesy of ZBD)

Bistable nematic devices

Despite their differences, all of the LC-based bistable devices that have been proposed make use of flat cells whose surfaces couple to the LC to frustrate the development of uniform molecular alignment. Bistability emerges when the nematic can satisfy the external constraints with (typically) two different configurations that cannot be transformed into each other by continuous rearrangement of the local alignment. These two states should be topologically distinct, so that the thermal energy cannot induce a state switch.

While the first bistable displays were based on special LC molecules, like ferroelectric LCs[5], or used phases with complex symmetry, like the smectic phase[6], the first generation of bistable devices based on NLCs was developed in the 90s by Durand and co-workers[7,8](see Fig. 1c). In that scheme, the frustration was obtained in a cell with slightly tilted planar parallel boundary conditions by doping the NLC with a small amount of chiral molecules[9] to induce a spontaneous twist distortion in the nematic ordering (chiral nematic phase). In this way, the NLC can match the surface conditions by adopting either a twisted or a slightly splayed configuration, which are both stable and long-lived. Hydrodynamic coupling to the LC director (the preferred direction of orientation) enables switching between the two states by using electric field (*E*) pulses with different shapes: slowly removing the electric field drives the nematic to the unwound, splayed state, while abruptly removing the field leads to the twisted state.

A second generation of chiral nematic-based bistable devices was developed in the late 90s[10-14] (see Fig. 1d). In this case, the boundary conditions and LCs were chosen so that a uniform helix across the cell spontaneously developed, with a pitch low enough to reflect

the illuminating light through a Bragg-like mechanism[1]. Applying an electric field parallel to the helix direction induces a transition to the so-called *focal conic* state, where the uniform helical order is disrupted, and helical arrangements develop locally in random orientations. In this state, the Bragg reflection is suppressed and the cell becomes rather transparent, letting the transmitted light be collected by an absorbing layer on the back of the device (Fig. 1d). Whether the system relaxes back in the reflecting uniform twist phase or remains stuck in the focal conic state again depends on the kinetics of the field removal. Fujitsu's FLEPia reader is based on this technology (Fig. 1f[15]), as well as the Binem display by Nemoptic.

Frustration, and therefore bistability, can also be induced through surface patterning. The zenithal bistable display (ZBD)[16-20], the most famous of this class of device, uses thin cells, where one surface has a complex morphology (such as the saw-tooth shape in Fig. 1e) and forces perpendicular molecular anchoring. A commercial example of this is the Epop display by ZBD, shown in Fig. 1g[21]. Here, once more, the LC has two possible long-lived states that can be switched using *E* pulses of different shapes. The different optical properties of the two states can be used in the design of bistable pixels, becoming light and dark when between crossed polarizers. Extensions of this concept to three-state cells have been also proposed[22].

The explanation of why the configuration shown in Fig. 1e is a stable state relies on an understanding of the topological defects, i.e., regions where the nematic ordering is not defined[1] (red and blue dots in the figure), which develop in the cell. As will be explained, the geometrical constraints of defects represent a fundamental descriptor of confined liquid crystals.

Memory effects in disordered nematics

A new perspective on the notion of topologically distinct metastable states is offered by nematics incorporated in micron-sized pores of solid matrices. This class of system is optically interesting because they are generally extremely turbid, but become clear when an electric field is applied. Optical turbidity, τ, represents a intensive property of the material, corresponding to the inverse mean free path that the photons can travel within the material before being scattered. A large turbidity indicates a short photon mean free path and thus a small transmitted intensity. The large turbidity of these systems is a consequence of the intrinsic birefringence of nematics and of the orientational disorder induced by their interactions with the surfaces of the host matrix. The confinement of NLC in micron-sized pores results in big spatial fluctuations of the refractive index on the length scale of optical wavelengths, a property that produces a large scattering cross section for light, as happens in white materials, like paper, fabric, and paint. By applying a strong enough electric field, orientational order is forced along the field direction, and the refractive index thus becomes more uniform and the scattering cross section decreases.

It was observed that some of these systems show memory effects[23-31]: after the electric field is removed, the light transmittance does not grow back to its original value (Fig. 2a). This means that the field-induced orientational order is partially recorded in the system. This memory can be erased by heating and cooling, transitorily melting the nematic order. From their study in the early 90s of nematics dispersed in polymer structures with different morphologies[25,26,28], Yamaguchi and co-workers showed that disconnected pores (such as in the scanning electron microscope photograph of Fig. 2c, schematized in Fig. 2e) do not yield significant memory effects. These effects are instead observed in (some) cases where the pores form a multiply connected structure in which the NLC alignment is continuously distorted, as sketched in Fig. 2f. In Fig. 2b the behavior of NLC embedded in polymeric matrices with disconnected (Fig. 2c) and connected (Fig. 2d) pores are compared by plotting the light transmittance of these structures during (full dots) and after (open dots) the application of an electric field as a function of the field amplitude[28]. In the interconnected structures, after the removal of the field, the transmitted intensity decreases only partially. It would thus be useful to maximize this effect and have materials that, once made transparent (or opaque) by an external field, would permanently preserve that state. The problem is that the amount of memory displayed by different structures is difficult to predict. Our research group has studied the behavior of nematics incorporated in the disordered porous cavities of Millipore filter membranes (Fig. 2h) or colloidal gels made of aggregated silica nanoparticles[29-32] (filled nematics, Fig. 2i). These structures differ in chemical composition, in morphology, and in their characteristic size. However, both confining structures lead to similar memories after the removal of E, as shown by the field dependence of the turbidity reported in Fig. 2g. By means of appropriate scattering models[33] the measured turbidity, τ, can be used to estimate the overall molecular orientational order of the LC within the porous network, as expressed by the nematic order parameter Q ($Q = 0$ indicates no ordering, while $Q = 1$ indicates perfect alignment)[1]. In the most relevant cases, a simple approximate linear dependence can be derived: $Q \approx 1 - \tau/\tau_0$, where τ_0 is the turbidity of the unperturbed system[31].
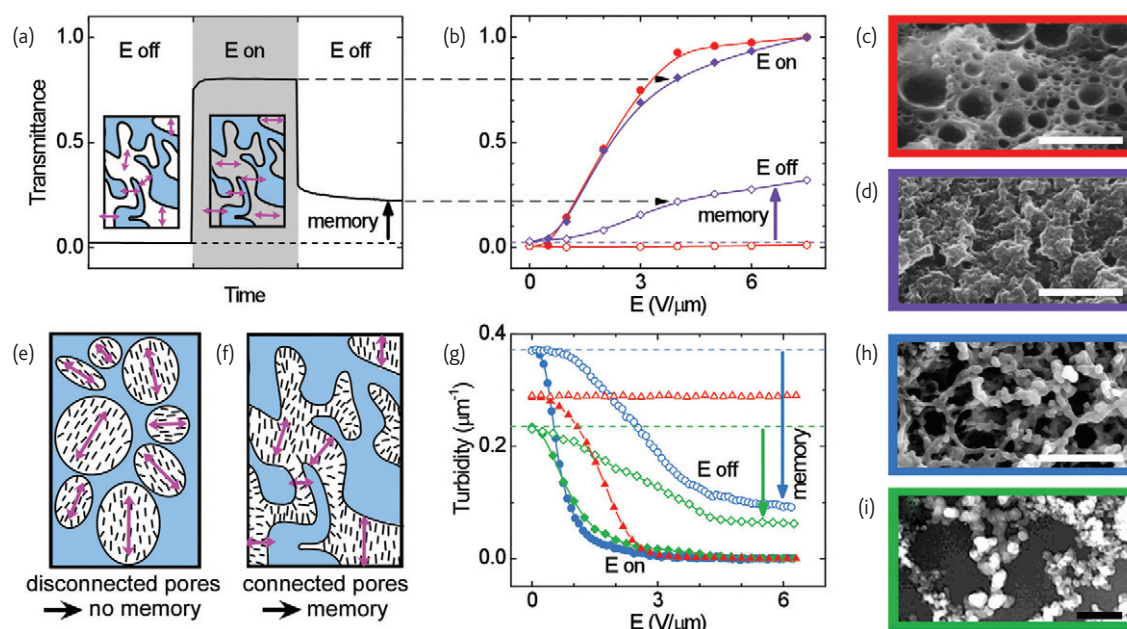

Fig. 2 Memory effects in disordered nematics. (a) Transmittance, T, as a function of the applied field. (b-d) Transmittance in polymer-dispersed nematics in (c, red) disconnected and (d, violet)connected cavities. (e, f) Schematics of NLC orientation in cavities. (g) Turbidity, τ, of nematics embedded in disconnected pores (red), in (h, blue) Millipore filters and (i, green) filled nematics. $\tau = -ln(T)/d$, d being the sample thickness. Scale bar in (c), (d), and (h) is 10 µm, and in (i) is 0.2 µm. (b-d) Adapted from[28]. (h) Courtesy of Dr M. Carpineti.

The memory effects described in Fig. 2 are scientifically interesting but not significant enough for applications. Given the complexity of the problem, the optimization of NLC memory on the basis of the structure of the microporous confining material has to be approached through 3D computer simulations. This strategy, which lets us *look inside* the structure of nematics in these complex environments, has recently led to new insights on the emergence of memory in these systems.

The secret ingredient: topological defect lines

As it turns out, memory is better understood when topological defects are included in the description of NLC confined in porous matrices. Defects are points or lines in the proximity of which the nematic order is lost[34,35]. Topological defects typically arise within the nematic fluid when boundary conditions do not allow the formation of uniform ordering. This phenomenon is exemplified in Fig. 3, which shows the necessity of a topological defect in a brick-made apse of a Romanesque church: the boundary conditions, i.e., the orientation of the bricks along the perimeter of the apse, cannot be smoothly joined with aligned bricks. In this condition, both in the apse (Fig. 3a and 3b) and in nematics[36] (Fig. 3c), a topological defect (red dot in the figure) is formed. Defects concentrate distortions, at the same time enabling the surrounding material to be locally ordered. In real 3D nematics, topological defects often develop in lines (Fig. 3d) that cannot terminate within the nematic bulk, and are thus typically closed in loops. In transient situations, the application of an external field leads to line defects expanding in plane defects, before nematic order reconstruction[37].

The role of topological defects in the behavior of nematics confined in complex geometries has been elucidated by computer simulation studies[38-40] based on the Lebwohl-Lasher (LL) spin lattice model[41,42] of nematic LCs. This is a simple approach in which nematic order develops in a system of freely orienting spins on a lattice as a consequence of their mutual interaction. A first set of LL-based simulations was performed by mimicking the effect of disordered and interconnected confinement by adding a strong and randomly oriented field acting on a randomly chosen fraction of the spins[43]. In this way, a portion of the spins is constrained in disordered orientations, as are the molecules in contact with the solid interface in real systems, while the rest of them try to find a compromise between the disordering forces and their "natural" orientation ordering. This *random-field* model is conceptually very simple and has demonstrated that nematics with random disorder are populated by a large number of defect loops, whose length and trajectory characterize the difference between the metastable states. In this approach, the system becomes rich with pinning sites for the defect lines. The outcome is a network of defects resembling a 3D "connect the dots" game, in which however the dots (i.e., the pinning sites) can be connected in a wide variety of ways (each corresponding to one of the multiple metastable states). The various options of connectivity can be switched by sufficiently strong external fields acting on the locally oriented nematic, which in turn is coupled to the geometry of the defect lines.

Random-field computer simulations have thus unraveled an essential and intriguing characteristic of NLCs confined in porous media. In addition to the "real" components of these hybrid materials (the porous matrix and NLC), a third, immaterial constituent is present
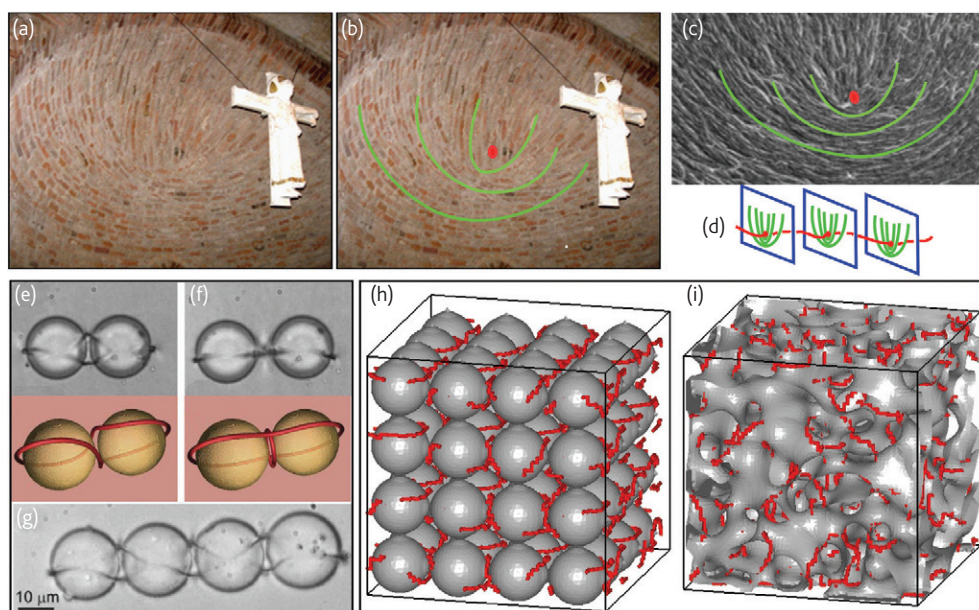

Fig. 3 Examples of topological defects. (a,b) Disclination defect in the apse of "Rotonda di san Lorenzo", Mantova, and (c) in an NLC: the molecular alignment is made visible by polymer bundles[36]. In 3D NLC, disclinations are arranged into (d, red line) lines which are found near microspheres (e, f, g) immersed in a NLC. (h,i) Topological defects are also predicted by computer simulations of NLC incorporated into bicontinuous regular or random lattices. (c) Courtesy of Dr I. Dierking. (e,f,g) Reprinted figure with permission from[45]. © 2007 by the American Physical Society. (h,i) Courtesy of Dr T. Araki.

in the system: the network of topological defect lines, which determine the variety of metastable states and their stability.

Crocheting complex structures with defect lines

The analysis of disordered nematics based on random-field models is interesting from a fundamental standpoint, but offers no tools to design real structures that would maximize multistability and memory effects. Inspiration about how to approach the problem from a different angle is presented by an independent set of experimental observations, theory, and computer simulations, showing how topological defects arise when smooth regular surfaces favoring perpendicular NLC alignment (i.e., no randomness) are inserted in a nematic. In particular, many studies have been devoted to NLC hosting microspheres[44-52]. Interestingly, even in the simple case of two spherical microinclusions, it is found that the overall topological constraints exerted by the combined surfaces on the NLC can be matched by more than one choice of defect line trajectory: the two states in Fig. 3e and Fig. 3f, are topologically distinct, although the energy barrier between the two metastable states is rather low. Topological defects can mediate colloidal assembly when more spherical inclusions are considered (Fig. 3g). A recent experimental study[51] has shown that it is indeed possible to tie and untie knots of defect lines around colloidal particles, thus showing that defect lines can be effectively treated as real objects and manipulated.

A recent LL-based computer investigation[53] has studied the topological state of nematics incorporated in bicontinuous solid structures having various geometries, both periodic and disordered (Fig. 3h and 3i). This analysis confirms that bicontinuous porous structures with perpendicular surface anchoring of the NLC molecules induce the formation of a large number of defect loops, a fraction of which encircle the solid portions.

A quantity which is commonly used to define topological states is the *topological charge, M*. More technically, a topological charge can be assigned to every topological defect and it represents the angle by which the nematic director "turns" around the defect, divided by 2π. In the example shown in Fig. 3b and 3c the nematic director makes a 180°

angle around the defect, therefore the topological charge is ½. Rigorous definitions of topological charge can be found elsewhere[54,55,34]. In the simple cases, for porous systems with perpendicular boundary conditions, the modulus of the topological charge equals the number of elementary defect loops. The amount of topological charge in a confined NLC depends on the symmetry of the porous network. This is demonstrated in a recent experimental and theoretical analysis[56] of the topological state of NLCs in porous networks such as the 3D cubic arrangement of cylindrical channels shown in Fig. 4a. By viewing these structures as a combination of elemental units as in a jigsaw puzzle, it can be shown that the number of defects (more rigorously expressed by the total topological charge) depends on the valence v of the nodes of the network, i.e., the number of channels merging in the vertices of the network (nodes of valence 3 and 4 are shown in Fig. 4b). For example, the prediction for a bicontinuous cubic structure (as the one of Fig. 4a), obtained by combining nodes of valence 6, is of two defect loops per unit cell. Ten years ago Kang and coworkers[57] studied NLCs in the interstitial spaces of a colloidal crystal of closed packed microspheres (face-centered-cubic lattice) with perpendicular anchoring. In order to calculate the topological charge for such a complex geometry, it is important to identify a relevant *unit node*, as the one sketched in Fig. 4d. In this structure, the prediction of reference 56 is of five elementary loops per unit cell. Similarly, with the formula reported in Fig. 4c, it is possible to calculate the topological charge per unit cell for lattices with various symmetries.

It is expected and found that NLCs in bicontinuous porous matrices are populated by defect lines that permeate the structure, adopting one of the many possible choices of trajectories. Many of these loops are stuck to their trajectories. Indeed, changing the path of loops that encircle solid handles of porous matrices as in Fig. 3h and 3i would require "cutting" the loops and reconfiguring large portions of the nematic order. This operation costs much more energy than is provided by the thermal noise, and gauges the magnitude of the energy barriers that separate the distinct configurations. Moreover, the presence of the solid structure makes these loops irreducible
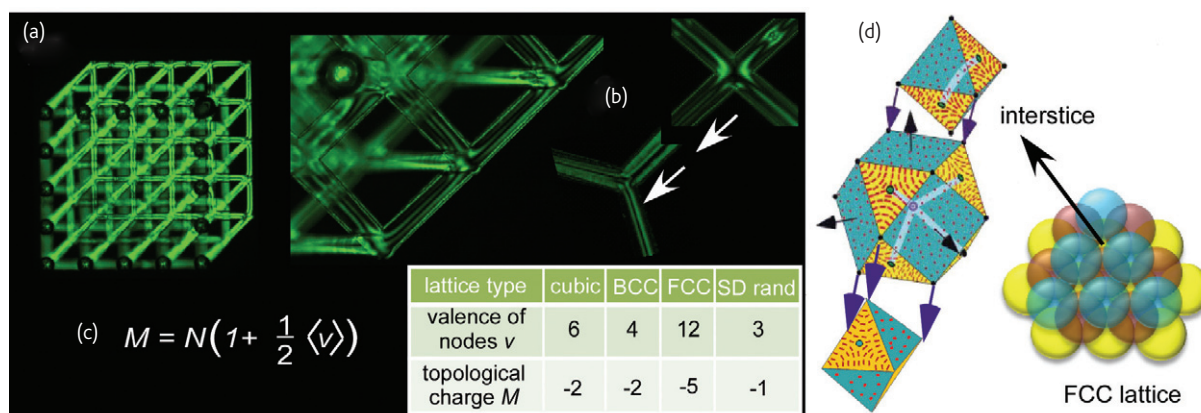

(c) $$M = N\left(1 + \frac{1}{2}\langle v\rangle\right)$$

lattice type	cubic	BCC	FCC	SD rand
valence of nodes v	6	4	12	3
topological charge M	-2	-2	-5	-1

Fig. 4 3D network filled with NLC. (a) Network of glass microfabricated channels (diameter 30 μm). (b) Detail of the structure and combinable elements of the structures. (c) Formula for topological charge and table with the topological charge of unit cells with various symmetries: cubic, body-centered-cubic (bcc), face-centered-cubic (fcc) lattices, and random porous network obtained by spinodal decomposition (SD rand)[56]. (d) An FCC-type structure made from closely packed spheres and detail of LC alignment in the interstice. Reprinted figure with permission from[57]. ©2001 by the American Physical Society.

by preventing them from contracting to point defects; quite different, for example, from defect loops around spheres that can slide along the sphere and contract to a point. The irreducible character of the loops combined with the importance of the energy barriers is the cause of the multistability of NLCs confined in smooth bicontinuous porous media.

The basic symmetry (random, cubic, hexagonal, random) of the porous matrices and their detailed morphology have relevant roles in determining the amplitude of the memory effects and in the kinetic response of these hybrid systems. Fig. 5 shows the trajectories of defect lines within porous media having periodic and random geometry, as obtained (i) by cooling the system into the NLC phase with no electric field applied (Figs. 5a and b), a condition in which the NLC is locally ordered but globally disordered, and, (ii) after the application and removal of an electric field (Figs. 5c and d). Figs. 5e and f show, for the two structures, the global orientational order of the NLC molecules, as expressed by the order parameter Q, before, during and after the application of the field. It is found that random porous media, such as those provided by Millipore filter membranes, have weak memory (the ordering forced by the field is largely lost as the field is removed) and very slow relaxations, reminiscent of a glassy behavior[31]. On the contrary, bicontinuous cubic matrices are found to maximize memory and minimize the response time. The comparative analysis of these two structures and their behavior indicates that the improved performances of the bicontinuous cubic structure are due to the optimized combination of symmetry and local curvature. The electric field forces defect loops to be localized along the black lines in Fig. 5h, i.e., where the pore surface is laying parallel to the field. As the field is removed, defects modify their paths to minimize the elastic energy of the nematic, typically moving close to the areas with the largest negative Gaussian curvature, marked by magenta lines in Fig. 5i. In the case of the bicontinuous cubic, the local curvature of the surface favors

the defect lines being held along the same paths where they are driven by the electric field, thus largely maintaining the alignment induced by the field.

How good could it get?

The performance of bicontinuous cubic matrices in terms of retaining memory are much better than those of the random porous network (see Fig. 5g) and better than other pore geometries[49]. From the simulation studies it appears that the topology and the geometry of the hosting matrix determines the memory properties of the NLC. The upcoming challenge is to experimentally realize porous materials with tailored geometries to be exploited in bistable devices. The recent improvement of 3D microfabrication technologies[53], such as soft lithography, self-assembly, femtosecond laser microfabrication, and two-photon polymerization are making the exploration of microconfined nematics progressively viable and enabling the downsizing of single pixels.

E-paper seems to be a suitable application for these composite materials. The ideal e-book visualization should have the characteristics of printed paper, be readable in all ambient lights, and permanently hold images until rewritten. Current LC technologies are not used for e-book applications because of their poor display in strong ambient light and their significant energy consumption. The low consumption of the new composite materials is granted by their multistability. Moreover, choosing the geometry appropriately also leads to a lowering of the threshold field that is needed to switch the device between its metastable states.

Confined NLCs also have significant potential in matching the other criteria. The readability of paper comes from its strong turbidity. Confined nematics are quite promising in this respect since they enable high levels of turbidity to be achieved. Specifically, the fact that turbidity is produced by the distortion of a highly birefringent uniaxial material, such as the
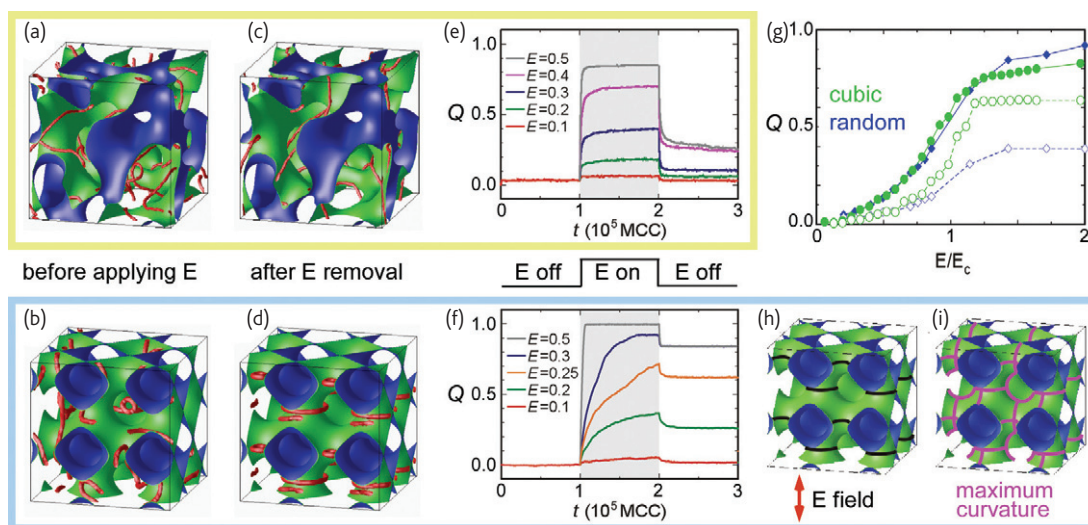

Fig. 5 Memory effects in (yellow box) random and (cerulean box) cubic porous structures (computer simulations). Defect lines (red) before (a,b) and after (c,d) field pulse. (e,f) Average molecular ordering, Q, evolving with the number of Monte Carlo cycles (MCC). (g) Q during (full symbols) and after (open symbols) field application vs field amplitude. The superior memory of the cubic structure is understood by comparing the defect trajectories in (h) high field to the (i) loci of largest negative Gaussian curvature. Adapted from[53].

nematic, allows values of turbidity of among the highest possible in any material to be reached[31]. Therefore cells of confined nematics as thin as a few tens of microns could provide the white state necessary for efficient visualization in ambient light illumination.

At the same time, the confined NLC-based device could be switchable from a transparent state to a turbid one. This can in principle be done using various strategies. One approach is to use electric fields perpendicular to the cell to induce alignment, and thus transparency, while using in-plane electric patterns to generate distortions. Another strategy is to employ dual-frequency materials, a promising development in NLC-based display technology[59,60]. The dielectric anisotropy of these materials changes sign with frequency, thus enabling switching between the transparent (axial alignment) and the scattering (degenerate planar alignment) states using the same electrodes.

The value of frustration and defects

In this article we discussed how confinement generally leads to a conflict between the long-ranged orientational ordering of nematic LC and the orientational constraints exerted on the molecules in contact with the surfaces of the porous matrix. This frustration of the NLC ordering results in the loss of a well-defined ground state, which is instead replaced by a multiplicity of metastable 3D patterns of alignment. In this way, metastability can be achieved by *functionalizing* the nematic via geometric confinement.

Quite interestingly, the behavior of these two-component hybrid materials formed by nematics in bicontinuous porous matrices is dominated by the behavior of a third component: topological defect lines. Their trajectories, their connectivity, and their interactions with the local curvature of the hosting matrix determine the characteristics of the metastable states, the energy required to switch between them, and the kinetic response of the system. "By nature we have no defects that could not become a strength" (J.W. Goethe)[61] . mt

REFERENCES

1. De Gennes, P. G., and Prost, J., *The Physics of Liquid Crystals*, Clarendon Press, Oxford (1993).
2. Schadt, M., *Annu Rev Mater Sci* (1997) **27**, 305.
3. Lu, R., *et al.*, *IEEE J Disp Tech* (2005) **1**, 3.
4. Hong, H., *et al.*, *J Disp Tech* (2007) **3**, 361.
5. Clark, N. A., and Lagerwall, S. T., *Appl Phys Lett* (1980) **36**, 899.
6. Coates, D., *et al.*, *J Phys D Appl Phys* (1978) **11**, 2025.
7. Durand, G., *Proc SPIE* (1996) **2949**, 2.
8. Dozov, I., *et al.*, *Appl Phys Lett* (1997) **70**, 1179.
9. Lee, S. H., *et al.*, *Appl Phys Lett* (2003) **82**, 4215.
10. Jeng, S. -C., *et al.*, *Opt Express* (2010) **18**, 22572.
11. Kim, K -H., *et al.*, *Opt Express* (2010) **18**, 16745.
12. Yang, D -K., *J Disp Tech* (2006) **2**, 1551.
13. Yang, D -K., *et al.*, *Annu Rev Mater Sci* (1997) **27**, 117.
14. Yao, I. -A., *et al.*, *Appl Phys Lett* (2009) **94**, 071104.
15. www.fujitsu.com/img/PR/2005/20050713-01.jpg
16. Bryan-Brown, G. P., *Proc SID 97* (1997) **28**, 37.
17. Bryan-Brown, G. P., *Nature* (1998) **392**, 365.
18. Jones, J. C. *et al.*, *Proc SPIE*, (2000) **3955**, 84.
19. Uche, C., *et al.*, *Liq Cryst* (2006) **33**, 697.
20. Jones, J. C., and Amos, R. M., *Mol Cryst Liq Cryst* (2011) **543**, 57.
21. http://www.zbdsolutions.com/.
22. Kim, J. H., *et al.*, *Nature* (2002) **420**, 159.
23. Jakli, A., *Mol Cryst Liq Cryst* (1994) **251**, 289.
24. Jain, S. C., and Rout, D. K., *J Appl Phys* (1991) **70**, 6988.
25. Yamaguchi, R., and Sato, S., *Liq Cryst* (1993) **14**, 929.
26. Yamaguchi, R., and Sato, S., *Jpn J Appl Phys* (1991) **30**, L616.
27. Glushchenko, A., *et al.*, *Liq Cryst* (1997) **23**, 241.
28. Yamaguchi, R., and Sato, S., *Jpn J Appl Phys* (1992) **31**, L254.
29. Bellini, T., *et al.*, *Phys Rev Lett* (2000) **85**, 1008.
30. Bellini, T., *et al.*, *Phys Rev Lett* (2002) **88**, 245506.
31. Buscaglia, M., *et al.*, *Phys Rev E* (2006) **74**, 011706.
32. Rotunno, M., *et al.*, *Phys Rev Lett* (2005) **94**, 097802.
33. Bellini, T., *et al.*, *Phys Rev E* (1998) **57**, 2996.
34. Kléman, M., *Rep Prog Phys* (1989) **52**,555.
35. Lavrentovich, O. D., and Kléman, M., *Phis Mag* (2006) **86**, 4117.
36. Dierking, I., *Polym Chem* (2010) **1**, 1153.
37. Ambrožič, M., *et al.*, *Phys Rev E* (2007) **75**, 031708.
38. Zhang, Z. P., and Chakrabarti, A., *Phys Rev E* (1995) **52**, 4991.
39. Chiccoli, C., *et al.*, *Mol Cryst Liq Cryst* (2010) **527**, 119.
40. Bellini, T., *et al.*, *Phys Rev E* (1996) **54**, 2647.
41. Lasher, G., *Phys Rev A* (1972) **5**, 1350.
42. Lebwohl, P. A., and Lasher, G., *Phys Rev A* (1972) **6**, 426.
43. Cvetko, M., *et al.*, *Liq Cryst* (2009) **36**, 33.
44. Muševič, I., *et al.*, *Science* (2006) **313**, 954.
45. Ravnik, M., *et al.*, *Phys Rev Lett* (2007) **99**, 247801.
46. Stark, H., *Phys Rep Rev Phys Lett* (2001) **351**, 387.
47. Poulin, P., *et al.*, *Science* (1997) **275**, 1770.
48. Araki , T., and Tanaka, H., *Phys Rev Lett* (2006) **97**, 127801.
49. Terentjev, E. M., *Phys Rev E* (1995) **51**, 1330.
50. Poulin, P., and Weisz, D.A., *Phys Rev E* (1998) **57**, 626.
51. Tkaleč, U., *et al.*, *Science* (2011) **333**, 62.
52. Čopar, S., and Žumer, S., *Phys Rev Lett* (2011) **106**, 177801.
53. Araki, T. *et al.*, *Nature Mater* (2011) **10**, 303.
54. Chandrasekhar, S., and Ranganath, G. S., *Adv Phys* (1986) **35**, 507.
55. Sonnet, A. M., and Virga, E. G., *Liq Cryst* (2010) **37**, 785.
56. Serra, F., *et al.*, *Soft Matter* (2011) doi: 10.1039/c1sm05813d.
57. Kang, D., *et al.*, *Phys Rev Lett* (2001) **86**, 4052.
58. Maselli, V., *et al.*, *Appl Phys Lett* (2006) **88**, 191107.
59. Golovin, A. B., *et al.*, *Appl Phys Lett* (2003) **83**, 3864.
60. Hsieh, C. T., *et al.*, *Opt Express* (2007) **15**, 11685.
61. *Von Natur besitzen wir keinen Fehler, der nicht zur Tugend [...] werden koennte*, from J. W. von Goethe, Wilhelm Meisters Wanderjahre I, 10.